# Mask, the *Drosophila* Ankyrin Repeat and KH domain-containing protein, regulates microtubule dynamics

Mingwei Zhu[1†], Daniel Martinez[1†], Jessie J. Guidry[2], Niles Majeste[1], Hui Mao[1], Sarah Yanofsky[1], Xiaolin Tian[1*] and Chunlai Wu[1]

[1]Neuroscience Center of Excellence, Department of Cell Biology and Anatomy, Louisiana State University Health Sciences Center, New Orleans, LA 70112, USA

[2]Proteomics Core Facility, and the Department of Biochemistry and Molecular Biology, Louisiana State University Health Sciences Center, New Orleans, LA 70112, USA

[†] These authors contributed equally

*Corresponding author

LSUHSC-NO, Neuroscience Center of Excellence

2020 Gravier St. STE.D

New Orleans, LA 70112

Phone: 504-568-2007

Email address: xtian@lsuhsc.edu

## Author Contribution

M.Z. and D. M. collected majority of the data. M.Z., C.W. and X.T. designed the experiments. J.J.G. designed and performed the mass spec analysis, N.M. performed the quantifications of microtubule length, H.M. and S.Y. provided technical supports. X.T. and C.W. prepared the manuscript.

## Abstract

Proper regulation of microtubule (MT) dynamics is vital for essential cellular processes and many neuronal activities, including axonal transport and synaptic growth and remodeling. Here we demonstrate that Mask negatively regulates MT stability and maintains a balanced MT length and architecture in both fly larval muscles and motor neurons. In larval muscles, loss of *mask* increases MT length, and altering *mask* genetically modifies the Tau-induced MT fragmentation. In motor neurons, loss of *mask* function reduces the number of End-Binding Protein 1 (EB1)-positive MT plus-ends in the axons and results in overexpansion of the presynaptic terminal at larval neuromuscular junctions (NMJ). *mask* shows strong genetic interaction with *stathmin* (*stai*), a neuronal modulator of MT dynamics, in regulation of axon transportation and synaptic terminal stability. The structure/function analysis on Mask suggests that Mask's action in regulating MT stability does not depend on the nucleotide-binding function of its KH domain. Furthermore, through a proteomic approach, we found that Mask physically interacts with Jupiter, an MT stabilizing factor. The MT localization of Jupiter in the axons inversely correlates with Mask levels, suggesting that Mask may modulate MT stability by inhibiting the association of Jupiter to MTs.

## Author Summary

Microtubules (MT) are part of the cytoskeleton of the cells that provides essential structural basis for critical processes and functions of the cells. A complex factors are required to orchestrate the assembly and disassembly of MT. Here we identified Mask as a novel regulator for MT dynamics in fruit flies. Mask negatively regulates MT stability. It shows prominent interplay with two important modulators of MT, Tau and *Stathmin* (*Stai*), both genes are linked to human neurodegenerative disorders. These findings not only support the role of Mask as a novel microtubule regulator, but also provide foundation to explore future therapeutic strategies in mitigating deficit related to dysfunction of Tau and Stathmin. Our further analysis on Mask protein demonstrate that Mask can physically interacts with another MT stabilizing factor named Jupiter. Jupiter can bind to MT, but its localization to the MTs in the axons is negatively affected by Mask, implying a possible underlying mechanism that Mask may modulate MT stability by inhibiting the association of Jupiter to MTs.

## Introduction

Terminally differentiated cells such as neurons and muscles use their microtubule (MT) network not for cell division but rather as architectural components essential for their shape and unique cellular functions. In addition to supporting the elongation of axons and change of dendritic morphology in neurons, MTs also act as direction-controlled railways for transporting materials and organelles between the cell body and pre- and post-synaptic sites (1). MTs can undergo cycles of dynamic assembly and disassembly (labile) or stay relative stable in a cell type- and developmental stage-dependent manner (2). For example, MTs in post-mitotic cells, such as neurons, are generally more stable than MTs in dividing cells; however, within a developing neuron, MTs at the axon growth cone are much more labile than MTs near the soma (3), and even in individual axons, MTs consist of domains that differ in stability (4). Recent studies suggest that both the stable and labile pools of MTs play essential roles for normal neuronal function. Furthermore, spacing among MTs and distance between MT ends were both shown to be critical for normal axonal transport (5, 6). Therefore, striking a balanced MT dynamic is key to maintaining MT-mediated cellular functions.

Many proteins and pathways have been identified as potential regulators of MT stability (2, 7). Among the major proteins controlling MT stability, Stathmin/SCG10 (superior cervical ganglion-10 protein) and Tau/MAPT are both MT-binding proteins that regulate multiple aspects of MT stability, including growth and shrinkage, as well as the transition between catastrophe and rescue. Both Stathmin and Tau are associated with diverse models of neurodegeneration, axon transport, and cancer (8-11). While *in vitro* studies of Stathmin-related proteins in mammals suggest that Stathmin promotes destabilization of MTs, studies of *stathmin* (*stai*) in fly neuromuscular junction (NMJs) showed that *stai* is required for MT stabilization, as well as axon

transport and NMJ stability (12, 13). The fly data is consistent with the finding that *stathmin* knockout mice show age-dependent axonopathy in both central and peripheral nervous systems, as well as defective motor axon outgrowth and regeneration (14, 15). Tau plays a multifaceted role in cell survival signaling. On the one hand, loss of Tau function or high levels of hyperphosphorylated Tau disrupts MT stability, leading to axonal transport defects in motor neurons and MT breakdown in larval muscles (16). On the other hand, hyperphosphorylated Tau aggregates form inclusion bodies that are associated with a variety of disorders collectively referred to as tauopathies, including Alzheimer's disease (Braak, 1991 Acta neuopathol). In animal models, such as rodents and fruit flies, overexpression of human Tau in the neuronal tissues leads to progressive neurodegeneration (17).

Mask is a 4001-amino-acid protein with a number of functional domains. It bears two Ankyrin Repeats: one Nuclear Export Signal (NES) and one Nuclear Localization Signal (NLS), as well as a C-terminal KH domain. The two Ankyrin repeat domains containing 15 and 10 tandem Ankyrin repeats likely coordinately facilitate the ability of Mask to associate with other proteins, according to the well-documented functions of the Ankyrin domains in mediating protein-protein interactions in eukaryotic cells (18). NES and NLS motifs may be required for shuttling Mask protein in and out of the nucleus. The KH domain is an evolutionarily conserved motif that is about 70 amino acids long, which was first identified in the human heterogeneous nuclear ribonucleoprotein K (19). KH domains bind RNA or single-stranded DNA (ssDNA) and are found in proteins that are associated with transcription, translation and mRNA stability regulation (20, 21). Recent studies showed that mutating the GXXG loop to GDDG in the KH minimal motif reduced the ability of KH domain to bind RNAs (22). The GXXG loop of Mask resides in amino acid 3053-3056 as GRGG, which is completely conserved between fly Mask

and human ANKHD1 (corresponding sequence 1710-1713). Mask plays an essential role in mitotic cells to regulate cell proliferation during development (23). It is a major component of the centrosome and nuclear matrix (24, 25), and a co-transcription factor of the Hippo pathway (26, 27). Also, its human homolog, ANKHD1, is expressed at relatively high levels in acute leukemia cells (28) and multiple myeloma cells (29). However, its function in post-mitotic cells, including neurons and muscle cells, is largely unknown. Here we show that Mask activity is required for balanced MT stability in two post-mitotic cell types and that *mask* interacts genetically with two MT-interacting proteins, Tau and Stathmin, whose dysfunctions are linked with human diseases.

## Results

### Mask negatively regulates MT length in larval muscles

Our previous studies of the putative scaffolding protein Mask demonstrated that overexpressing Mask ameliorate the degeneration of photoreceptors caused by overexpressing Tau in adult fly eyes (30). This finding prompted us to explore further potential interactions between Mask and Tau in the context of microtubule (MT) morphology, given the fact that Tau is a well-studied MT-binding protein. We first examined the MT morphology in *mask* loss-of-function mutants. Interestingly, we found that, in the larval body wall muscles, the MTs in *mask* null mutants are substantially longer than those in wild type control, particularly in the area surrounding the muscle nuclei (Fig. 1AB). Such a phenotype is fully rescued by introducing the UAS-Mask transgene back to the *mask* mutant larval muscles (Fig. 1AB). To further confirm this finding, we introduced *UAS-mask RNAi* to the wild type larval muscle and found that *mask* knockdown also increased muscular MT length (Fig. 1). These data suggested that normal Mask function in larval muscles is to restrain MT length.

### Loss of *mask* function suppresses, while upregulation of Mask enhances Tau-induced MT breakdown and toxicity in fly muscles

Next, we examined the interplay between Mask and Tau in regulating the MT network in larval muscles. We co-expressed human Tau protein with *UAS-control*, *UAS-mask RNAi*, or *UAS-Mask* and analyzed the MT length under each condition. Overexpression of human Tau in fly muscles causes severe destruction of the MT network, and residual MT becomes short and punctate (Fig. 1 C), which is consistent with a previously reported study on human Tau overexpression in fly

muscles (16). Co-expression of *mask* RNAi with Tau substantially increases MT length, while co-expression of UAS-Mask with Tau further devastates the MT network – MT almost only exists in bright rod-shaped puncta (Fig. 1C,D).

Mask regulates presynaptic terminal growth in neuromuscular junctions

We next analyzed the neuronal functions of *mask* at the fly larval NMJ. We found that *mask* null mutant ($mask^{10.22/df}$) NMJs show expanded presynaptic terminal growth reflected by an increased number of bouton, synaptic span, and number of branching points (Fig. 2AB). Such a morphological defect is due to loss of function of *mask* in the presynaptic motor neurons. First, pan-neuronal or ubiquitous expression, but not muscle (postsynaptic) expression, of UAS-Mask rescues the NMJ overgrowth phenotype in *mask* null mutants (Fig. 2AB). Second, neuronal knockdown of *mask* using a UAS-*mask* RNAi causes similar NMJ expansion as *mask* mutants (Fig. 2AB). Together these data demonstrate that neuronal Mask is required for controlling normal NMJ expansion in a cell-autonomous manner. Many genes and pathways were identified to regulate the presynaptic terminal size. To investigate whether neuronal Mask regulates presynaptic expansion through its function in regulating MT dynamics, we analyzed the number of MT plus-ends in the segmental nerve using an MT plus-end tracking protein End-Binding Protein 1 (EB1) (31). Neuronal knockdown of *mask* significantly reduced the number of EB1-GFP puncta comparing with control (Fig. 2CD), suggesting that loss of *mask* promoted elongation of MT in the axonal MT bundles.

*mask* and *stathmin* genetically interact with each other to regulate morphology and structural stability of NMJs.

To further investigate Mask's action in regulating MT elongation in neurons, we tested genetic interaction between *mask* and a well-established modulator of MT stability in neurons – *stathmin*. Loss of *stathmin* causes severe destabilization of MT in motor neurons, resulting in axonal transport defects, especially in the posterior segments, as well as premature loss of presynaptic structure at the nerve terminals (called "footprint" phenotype in *Drosophila* neuromuscular junctions). We found that the presynaptic NMJ expansion observed in *mask* mutant NMJs is completely suppressed in the *stai/mask* double mutant NMJs (Fig. 2AB). Similarly, the NMJ expansion phenotype induced by neuronal knockdown (RNAi) of *mask* can be partially suppressed by heterozygous *stai* mutation, and completely suppressed by homozygous *stai* mutation (Fig. 3AB), suggesting a strong genetic interaction between the two genes. In addition, *mask* loss of function can also reversely suppress neuronal defects caused by loss of *stai*. We found that both the footprint phenotype and the axonal transport defect of *stai* mutants are partially suppressed by neuronal knockdown of *mask*, and completely suppressed by *mask* null mutant (Fig. 3CD), suggesting the ability of enhanced MT stability in *mask* loss of function to compensate the impaired MT stability caused by loss of *stai*. These data strongly support that, when together, *mask* and *stai* antagonize each other in their action toward MT stability, and that *mask* regulates normal NMJ expansion by controlling MT stability.

Loss-of-function of *mask* results in elevated MT polymerization

Our morphological and genetic analyses suggested that normal function of *mask* is to restrain MT length. To further confirm this notion, we directly analyzed the rate of Tubulin polymerization in the cell lysates of wild type or *mask* knockdown larval muscles. We found that reducing Mask levels does not alter the total Tubulin concentration in muscle homogenates (Fig.

177 4A). In the presence of high-concentration (100 μM) taxol (a microtubule stabilization chemical),
178 Tubulin proteins in both control and mask *knockdown* lysates exist as polymerized forms as they
179 are detected exclusively in the pellet after ultracentrifugation (Fig. 4A). In the presence of low-
180 concentrations taxol (0.1 μM), more Tubulin proteins were detected in the supernatant fraction
181 (Tubulin monomer) than the pellet fraction (polymerized Tubulin) after ultracentrifugation.
182 However, the pellet from *mask*-knockdown muscle lysate contains significantly more
183 polymerized Tubulin than that from the control lysate (Fig. 4AB). These data suggest that loss of
184 *mask* activity in the cell lysate results in a condition that promotes MT polymerization.

185 Structure and function analysis of Mask for its action in modulating MT stability

186 In order to determine the domain requirement for Mask's functions, we generated UAS-Mask
187 transgenes that carry GRGG to GDDG mutation in their KH domain (named UAS-Mask-KH).
188 We also generated UAS-Mask deletion transgenes that lack either N- or C-terminal portions of
189 the protein (depicted in Fig. 5A). One resulting transgene contains the two Ankyrin repeats
190 (named Mask-ANK), and the other resulting transgene lacks the N-terminal portion of Mask and
191 contains the NES, NLS, and KH domains (named KH-Only).

192 We first expressed the mutant *mask* transgenes in the larval muscles in the *mask* null
193 mutants and confirmed that they express with predicted molecular weight and at levels
194 comparable to or higher than that of the wild type *mask* transgene (Fig. 5A). We then specifically
195 expressed those transgenes in either larval muscles or neurons to examine the abilities of these
196 transgenes to rescue the *mask* mutant defects in MT length in the muscle and the NMJ expansion
197 phenotype at the larval neuromuscular junctions, respectively. We found that the UAS-Mask-KH
198 transgene rescues *mask* mutant MT elongation in muscles (Fig. 5BC) and NMJ expansion at the

NMJs (Fig. 5DE) to a level that is comparable to wild type UAS-Mask transgene. These results suggest that the function of Mask KH domain is not required for Mask's action in regulating MT stability and presynaptic terminal expansion. However, neither UAS-Mask-KH-Only nor UAS-Mask-ANK deletion transgenes rescue *mask* mutant phenotypes in the larval muscles or at the neuromuscular junctions (Fig. 5B-E). In addition, expression of either UAS-Mask-KH-Only or UAS-Mask-ANK in wild type fly muscle causes pupal lethality similar to *mask* knockdown in muscle (data not shown), suggesting a dominant-negative effect. Such a dominant-negative effect indicates that the two truncated Mask proteins are likely folded and retain part of Mask activity, such as protein-protein interaction. The fact that the two Ankyrin repeat domains are not sufficient enough to rescue *mask* mutant defects suggests that the Mask C-terminal 1132 amino acid region, including Mask KH domain, is required for the intact Mask activity.

To understand the mechanism of *mask*-mediated regulation of MT stability, we set off to identify *in vivo* protein binding partners of Mask using the proximity labeling method, a unique technique in screening for physiologically relevant protein interactions in living cells (32, 33). By tagging the protein of interest with the promiscuous biotin ligase, these proteins can biotinylate proximal endogenous proteins *in vivo* in living cells. We generated UAS-based *mask* transgenes that harbor an N-terminal TurboID tag (34). We then expressed TurboID-Mask in fly brains using a pan-neuronal Gal4 driver Elav-Gal4 and raised the flies in Biotin-containing food. In parallel, we also raised Elav-Gal4-only flies in Biotin-containing food and used these flies as the control for baseline level biotinylation. We dissected ~300 larval brains from each group and performed affinity purification of biotinylated proteins using streptavidin-beads according to the established protocol (32, 33). Final elutes from this affinity purification were then analyzed through shotgun proteomics. Jupiter, an MT-associated protein, was identified as a Mask-binding

222 protein (ratio of TurboID-Mask vs. control: 1.6). To confirm the physical interaction between
223 Jupiter and Mask, we expressed mCherry-Jupiter in either fly muscles or fly brains, and
224 performed Co-IP experiments. In larval brain lysates, mCherry-Jupiter co-precipitates with
225 endogenous Mask, suggesting that Jupiter is a Mask-interacting protein (Fig. 6A).

226 Previous studies suggested that Jupiter may promote the stabilization of MT (35). Next,
227 we examined how Mask-Jupiter interaction could impact MT stabilization. We co-expressed
228 UAS-mCherry-Jupiter with UAS-control RNAi, mask RNAi or UAS-Mask in the fly brain and
229 found that total mCherry-Jupiter expression levels are not altered by gain or loss of *mask* levels
230 (Fig. 6B). However, Jupiter localization in both the segmental nerve (Fig. 6C, D) and NMJs (Fig.
231 6E, F) is substantially enhanced by *mask* loss-of-function, and it is significantly reduced by Mask
232 overexpression. We did not detect MT localization of either endogenous or transgenic Mask
233 proteins; rather, Mask proteins localize in the neuronal cell bodies surrounding the nuclei (data
234 not shown). The inversely related Jupiter's association with MT and the abundance of Mask
235 proteins suggests that Mask prevents Jupiter from localizing to MTs. The strong physical
236 interaction between Mask and Jupiter proteins and the non-MT localization of Mask suggest that
237 Mask prevents Jupiter from localizing to the MT by sequestering Jupiter protein away from MTs.

238 **Discussion**

239 The characteristics of MT organization and dynamics are cell-type specific. In non-neuronal cells,
240 MTs are labile and undergo frequent growth and shrinkage due to dynamic instability (36). In
241 neurons, MTs are generally more stable than MTs in dividing cells, although recent studies
242 indicate that there are also abundant labile MT fraction in neurons, especially in developing
243 neurons, and that a balance between labile and stable MT fractions contribute to normal neuronal

functions (4). A key MT-mediated neuronal function is axonal transport. Recent *in vivo* imaging studies of *C. elegans* motor neurons showed that the tiling of the MT fragments in axons is tightly regulated, and such intrinsic MT organization provides structural basis for efficient cargo transportation along the axons (6).

Decades of studies demonstrated that MT dynamics are tightly regulated by a number of mechanisms including GTP/GDP ratio, post-translational modification of MT, as well as a vast array of MT-stabilizing, MT polymerizing and depolymerizing, and MT-severing proteins. Our studies identify Mask as a novel regulator of MT stability that controls normal neuronal morphology during development and modulates MT dynamics under pathological conditions that are related to *stai* and Tau. Loss of *mask* resulted in elongated MTs in larval muscles and presynaptic over-expansion at the fly larval NMJs, a possible consequence of over-stabilization of MT as this phenotype is strongly suppressed by *stai*-induced MT destabilization (Fig. 2AB, Fig. 3AB), and that this phenotype is associated with increased density of Jupiter-mCherry on the axonal MTs (Fig. 6CD).

The function the Mask in regulating MT stability is further supported by its genetic interactions with *stathmin* and Tau. Previous studies on the effects of overexpressing human Tau in fly muscles showed that these ectopic Tau proteins are hyperphosphorylated and cause reduced MT density and enhanced fragmentation, similar to the finding in AD patients and mouse models (16). We found that Mask is capable of modulating the Tau-induced MT fragmentation in that loss of Mask enhances, while gain of Mask reduces MT length. Neuronal Stathmin family proteins are regulators of MT stability, and perturbation of Stathmin expression impacts neuronal development, plasticity, and regeneration (37). *Drosophila stathmin* mutations

cause severely disrupted axonal transport and presynaptic nerve terminal stabilization at the larval NMJs, likely due to impaired integrity of the MT network (12, 13). Knocking out mammalian STMN2, also known as SCG10, results in defects in axon outgrowth and regeneration (15). We found that loss of *mask* in neurons suppresses *stai*-induced axon transport and NMJ development phenotype in a dose-dependent manner (Fig. 3C-E), suggesting that Mask antagonizes the action of Stathmin in regulating MT stability. These data also suggested that defective homeostasis of MT network under pathological conditions can be restored by manipulating Mask levels in defined cell types.

We previously reported that Mask promotes autophagy in fly larval muscles (30). We then ask whether the ability of Mask to modulate Tau-induce MT fragmentation is a result of its potential ability to regulate abundance of the human Tau protein driven by the GAL4-UAS expression system in fly larval muscles. In line with the function of Mask to promote autophagic degradation, the levels of ectopic human Tau protein were significantly reduced when co-expressed with Mask, and it is substantially increased when co-expressed with *mask* RNAi (Fig. S1). In addition, Tau proteins in *mask* knockdown muscles start to form aggregated puncta, possibly due to the elevated levels of the Tau protein. Overexpressing Tau in the muscles causes the developing animals to die at the pupal stages, and knocking down *mask* suppresses the lethality (data not shown). These findings suggest that the formation of the Tau aggregates does not directly correlated with the toxicity caused by Tau in the muscles. The toxicity likely is primarily caused by severe MT fragmentation induced by Tau expression. MT fragmentation induced by Tau does not seem to be correlative to Tau protein levels, as co-overexpressing Mask with Tau not only significantly reduces the levels of the exogenously expressed Tau protein (Fig S1) but also potently enhances MT fragmentation (Fig. 1). These findings suggests that

289 dysregulation on Tau may cause defects in MT organization that is independent to the toxicity
290 induced by Tau aggregates.

291 Our loss-of-function studies demonstrated that *mask* is required for normal MT
292 organization in both neurons and muscles. However, overexpression of Mask reduces MT length
293 only under a sensitized background where human Tau induces severe MT fragmentation, but not
294 under an otherwise wild type background, indicating that Mask is not sufficient to drive
295 significant change in MT dynamics, and other co-factors may be required for such a gain of
296 function effect. Mask is a large scaffolding protein containing two ankyrin repeats at its N-
297 terminal and a KH-domain at its C-terminal. Ankyrin-repeats-containing proteins were
298 implicated in the regulation of MT dynamics. A designed ankyrin repeat protein was shown to
299 bind to the β-tubulin surface exposed at MT plus-ends with high affinity and cap MT elongation
300 (38). Two isoforms of *Drosophila* Ankyrin2, Ank2-L and Ank2-XL, regulate MT spacing in
301 conjunction with Futsch, and therefore control axon caliber and transport (39). The KH-domain,
302 on the other hand, may mediate Mask's action in regulating RNA alternative splicing (40) as
303 well as transcription through the HIPPO pathway (26, 27). Our structure/function studies of
304 Mask functional domains suggested that the two ankyrin repeats domains of Mask are crucial for
305 Mask's ability to negatively regulate MT elongation/stabilization, although themselves alone are
306 not sufficient to substitute Mask's action in modulating MT dynamics, and that the C-terminal
307 portion of protein, including the entire KH domain of Mask, is indispensable for Mask-mediated
308 regulation on MT dynamics. Together these data support the notion that Mask regulates MT
309 through protein-protein interactions, but not through its capacity to regulate alternative splicing
310 or transcription. Through the proximity labeling (BioID) approach, we identified Jupiter as one
311 of the Mask-interacting proteins and showed that manipulating Mask levels alters the MT

localization of Jupiter. One possible interpretation is that Mask, as a non-microtubule associated protein, physically interacts/sequesters Jupiter and prevents it from promoting MT polymerization and stability, and therefore, helps achieve a balance in MT dynamics. However, given that the precise function of Jupiter remains unclear, our current data could not exclude the possibility that the changes in the levels of MT localization of Jupiter directly correlates with the amount of the stabilized MT present in the dynamic pool, as Jupiter may preferentially bind to stabilized MT.

## Materials and Methods

*Drosophila strains, transgenes and genetics*

Flies were maintained at 25°C on standard food. The following strains were used in this study: $mask^{10.22}$ (23), $mask^{Df317}$, UAS-Jupiter-mCherry (41), BG380-Gal4 (neuron specific) (42), MHC-Gal4 (muscle specific), 24B-GAL4 (muscle-specific), DA-Gal4 (Ubiquitous), UAS-control-RNAi (P{TRiP.JF01147}), UAS-*mask*-RNAi (P{TRiP.HMS01045}) from the Bloomington stock center. Generation of the full-length wild type *mask* cDNA was previously described (43). This cDNA was used to generate pUAST-TurboID-Mask (34) and modified *mask* cDNA, including pUAST-Mask-KH, pUAST-GFP-Mask-KH-Only, pUAST-Mask-Ank. All transgenic fly lines were generated by BestGene Inc. (Chino Hills, CA, USA).

*Western blots*

Western blots were performed according to standard procedures. The following primary antibodies were used: mouse anti-β-Tubulin (1:1,000, E7) mouse anti-Alpha-Actin (1:1000, JLA20 ) from Developmental Studies Hybridoma Bank; rabbit anti-Mask (1:2,000) (23), mouse anti-mCherry antibody (1:1000, 1C51, NBP1-96752 Novus Biologicals), and rabbit anti-GFP

(1:1000, A11122, Invitrogen). All secondary antibodies were used at 1:10,000. Data were collected using Luminescent Image Analyzer LAS-3000 (FUJIFILM) and quantified using Multi Gauge (FUJIFILM).

*Immunocytochemistry*

Third instar larvae were dissected in ice-cold PBS and fixed in 4% PFA for 30 min. The fixed tissues were stained following standard procedures. Rabbit anti-MASK antibody (23) was pre-absorbed with *mask* mutant tissues and then used at 1:1000. The other primary antibodies used were: mouse anti-DLG, anti-Futsch and anti-β-Tubulin antibodies are from Developmental Studies Hybridoma Bank, rabbit anti-DVGlut (44), rabbit anti-GFP (A11122, Invitrogen) at 1:1000, rabbit anti-mCherry (632496, Clontech) at 1:1000, mouse anti-Acetylated Tubulin (T6793, Sigma), mouse anti-Tau (12-6400, Invitrogen) at 1: 1000. The following secondary antibodies (from Jackson ImmunoResearch ) were used: Cy3-conjugated goat anti-rabbit IgG at 1:1000, Dylight-488-conjugated anti-mouse IgG at 1:1000, and Alexa-Fluor-647-conjugated goat anti-HRP at 1:1000.

*Confocal imaging and analysis*

Single-layer or z-stack confocal images were captured on a Nikon (Tokyo, Japan) C1 confocal microscope. Images shown in the same figure were acquired using the same gain from samples that had been simultaneously fixed and stained. For quantification of microtubule length, z-stack confocal images of microtubule in larval muscle 6/7 in segment A2 were double-blinded, IMARIS software (Bitplane, Inc) was used to quantify average MT length in randomly selected muscle areas.

*Quantification of microtubule length in fly larval muscles*

The microtubule length was measured using IMARIS 9.2.1 imaging software. A 80 µm X 80 µm (1024X1024 pixel resolution) sized image for muscle 6 with step size 0.15 µm covering the entire depth of muscle volume that contains the microtubule network was used in the analysis. In each image, two areas of 30 x 30 µm were selected for quantification. For each randomly chosen area, 100 +/-50 tracing were performed, total number for each muscle sample is on average 250 filaments. In the 3D image, each microtubule was traced manually to ensure the precise tracing. Switching between 3D View to Slice is often used to properly follow microtubules that may seem to cross with other MTs in close proximity.

*Fractionation of Tubulin*

Fractionation of β-tubulin was performed as described by Xiong *et al.* with minor modifications (16). Larval muscles of 20 larvae from each genotype were dissected in PBS at room temperature (RT). These muscles were immediately homogenized in 300 ul lysis buffer (150mM KCl, 2mM $MgCl_2$, 50mM Tris, pH 7.5, 2mM EGTA, 2% glycerol, 0.125% Triton X-100, protease inhibitor cocktail) containing either 100 µM or 100 nM Taxol. After incubating for 10 min at RT, the homogenates were centrifuged at 1,500 X g for 5 minutes at RT to remove cellular debris. A small aliquot of the supernatant of each sample was collected to analyze the total β-Tubulin level. The remaining supernatant was ultra-centrifuged at 100,000 g for 30 minutes. After ultracentrifugation, each supernatant and pellet were separated and analyzed by SDS-PAGE and western blots.

*Generation of UAS-TurboID-Mask transgene*

The TurboID fragment was amplified by PCR using the V5-TurboID-NES-pCDNA3 plasmid (Addgene 107169) as the template. Two PCR primers were used: forward primer-

5'atctGAATTCatgggcaagcccatccccaa3'; and reverse primer-5'actcAGATCTgctgcctccgcctcccgatccgcctccgccctgcagcttttcggcagacc3'. The resulting fragment no longer contains the NES signal, while at the time includes an EcoRI site at the 5' end, a BglII site at the 3' end, and a linker sequence (GlyGlyGlyGlySerGlyGlyGlyGlySer). This fragment was subsequently cloned into the pGEM T-easy vector (Promega), then excised out with EcoRI and BglII and cloned into the pUAST plasmid, resulting in the plasmid vector "pUAST-TurboID".

An 11kb Mask sequence was excised out with BglII and XbaI from the pUAST-Mask plasmid (43) and ligated with the pUAST-TurboID vector to generate an intermediate construct. A 1.2kb Mask fragment with BglII ends was then ligated with this intermediate construct to generate the final pUAST-TurboID-Mask plasmid. The generation of the transgenic flies was aided by Bestgene, Inc.

*Purification and enrichment of biotinylated proteins*

The procedures for the purification and the enrichment of biotinylated proteins was adapted from (32). The TurboID-Mask transgene was expressed in all neurons under the control of the elav-Gal4 driver. 300 fly larval brains were dissected and homogenized in 1000ul lysis buffer (2M urea in 50 mM Tris·Cl pH 7.4, 1× protease inhibitor, 1 mM dithiothreitol (DTT), and 1% TritonX-100). After 5 minutes of incubation at room temperature, the homogenate was centrifuged at 16,500xg at 4˚C for 10 minutes. The biotinylated proteins were then pulldown by incubating the supernatant with prewashed 100ul of Magnabind Streptavidin beads (Invitrogen) over night at 4˚C. After rinsing with the lysis buffer for 4 times and twice with RIPA buffer (50 mM Tris pH 8, 150 mM NaCl, 0.1% SDS, 0.5% sodium deoxycholate, 1% Triton X-100, 1×

protease inhibitor cocktail (Sigma-Aldrich),1 mM PMSF), the beads are ready for proteomic analysis via LC-MS.

*Liquid Chromatography-Mass Spectrometry (LC-MS)*

The procedure was adapted from (34). After several washes in 50mM Tris, pH 7.5 containing 2M Urea, beads and bound biotinylated proteins were incubated with 0.5ug trypsin in 50mM Tris, pH 7.5/2M Urea for 1 hour with shaking. This step was repeated for a second 15-minute period. These supernatants were pooled, the cysteines were reduced during a 1 hour incubation at 55°C with 2ul of 500mM tris(2-carboxyethyl)phosphine, and subsequently alkylated with a 30-minute incubation with 5ul of 375mM Iodoacetamide in the dark. An additional 0.5ug of trypsin was added for an overnight incubation at room temperature.

The next day, samples were acidified by the addition of Trifluoroacetic acid until 0.5%, and then trypsinized peptides were purified using C18 tips (Thermo). The eluted peptides were dried to completion until ready for LC-MS analysis.

The samples were run on a Dionex U3000 nano flow system coupled to a Thermo Fusion mass spectrometer. Each sample was subjected to a 65-minute chromatographic method employing a gradient from 2-25% Acetonitrile in 0.1% Formic Acid (ACN/FA) over the course of 25 minutes, from 25 to 35% ACN/FA for an additional 10 minutes, from 35 to 50% ACN/FA for an additional 4 minutes, a step to 90% ACN/FA for 4 minutes and a re-equilibration into 2% ACN/FA. Chromatography was carried out in a “trap-and-load” format using a PicoChip source (New Objective, Woburn, MA); trap column C18 PepMap 100, 5um, 100A and the separation column was PicoChip REPROSIL-Pur C18-AQ, 3um, 120A, 105mm. The entire run was 0.3ul/min flow rate. Electrospray was achieved at 1.9kV

MS1 scans were performed in the Orbitrap utilizing a resolution of 240,000. And data dependent MS2 scans were performed in the Orbitrap using High Energy Collision Dissociation (HCD) of 30% using a resolution of 30,000.

Data analysis was performed using Proteome Discoverer 2.3 using SEQUEST HT scoring. The background proteome was Drosophila melanogaster (SwissProt TaxID 7227, version 2017-07-05, downloaded on 01/19/2018). Static modification included carbamidomethyl on cysteines (=57.021), and dynamic modification of methionine oxidation (=15.9949). Parent ion tolerance was 10ppm, fragment mass tolerance was 0.02Da, and the maximum number of missed cleavages was set to 2. Only high scoring peptides were considered utilizing a false discovery rate (FDR) of 1%. Label Free Quantitation was performed on individual sample files and quantitative ratios were compared to control samples.

*Statistical analysis*

Statistical analysis was performed, and graphs were generated in Origin (Origin Lab, Northampton, MA). Each sample was compared with other samples in the group (more than two) using ANOVA, or with the other sample in a group of two using T-test. All histograms are shown as mean ± SEM. The n numbers of each statistical analysis are indicated in the graph.

438

439 **Acknowledgments**

440

441 We would like to thank Michael Simon for the *mask* mutant alleles and the anti-Mask antibodies,
442 Chris Doe for the UAS-Jupiter-mCherry transgene, the Bloomington Stock center for other fly
443 stocks, and Developmental Studies Hybridoma Bank, created by the NICHD of the NIH and
444 maintained at The University of Iowa, Department of Biology, Iowa City, IA 52242, for
445 antibodies. We also thank Liz McGehee for editorial assistance. This work is supported by a
446 Start-up fund from LSUHSC to X.T. and an ALS Association Grant (18-IIA-414) to C.W. The
447 Proteomics Project described was supported by a grant from the National Institute of Health
448 Grant P30 GM103514.

## References

1. Kapitein LC, Hoogenraad CC. Building the Neuronal Microtubule Cytoskeleton. Neuron. 2015;87(3):492-506.
2. van der Vaart B, Akhmanova A, Straube A. Regulation of microtubule dynamic instability. Biochem Soc Trans. 2009;37(Pt 5):1007-13.
3. Hur EM, Saijilafu, Zhou FQ. Growing the growth cone: remodeling the cytoskeleton to promote axon regeneration. Trends Neurosci. 2012;35(3):164-74.
4. Baas PW, Rao AN, Matamoros AJ, Leo L. Stability properties of neuronal microtubules. Cytoskeleton (Hoboken, NJ). 2016;73(9):442-60.
5. Hahn I, Voelzmann A, Liew Y-T, Costa-Gomes B, Prokop A. The model of local axon homeostasis - explaining the role and regulation of microtubule bundles in axon maintenance and pathology. Neural Development. 2019;14(1):11.
6. Yogev S, Cooper R, Fetter R, Horowitz M, Shen K. Microtubule Organization Determines Axonal Transport Dynamics. Neuron. 2016;92(2):449-60.
7. Bowne-Anderson H, Hibbel A, Howard J. Regulation of Microtubule Growth and Catastrophe: Unifying Theory and Experiment. Trends in cell biology. 2015;25(12):769-79.
8. Rossi G, Redaelli V, Contiero P, Fabiano S, Tagliabue G, Perego P, et al. Tau Mutations Serve as a Novel Risk Factor for Cancer. Cancer research. 2018;78(13):3731-9.
9. Tararuk T, Ostman N, Li W, Bjorkblom B, Padzik A, Zdrojewska J, et al. JNK1 phosphorylation of SCG10 determines microtubule dynamics and axodendritic length. J Cell Biol. 2006;173(2):265-77.
10. Wen HL, Lin YT, Ting CH, Lin-Chao S, Li H, Hsieh-Li HM. Stathmin, a microtubule-destabilizing protein, is dysregulated in spinal muscular atrophy. Human molecular genetics. 2010;19(9):1766-78.
11. Strang KH, Golde TE, Giasson BI. MAPT mutations, tauopathy, and mechanisms of neurodegeneration. Laboratory investigation; a journal of technical methods and pathology. 2019;99(7):912-28.
12. Graf ER, Heerssen HM, Wright CM, Davis GW, DiAntonio A. Stathmin is required for stability of the Drosophila neuromuscular junction. J Neurosci. 2011;31(42):15026-34.
13. Duncan JE, Lytle NK, Zuniga A, Goldstein LS. The Microtubule Regulatory Protein Stathmin Is Required to Maintain the Integrity of Axonal Microtubules in Drosophila. PloS one. 2013;8(6):e68324.
14. Liedtke W, Leman EE, Fyffe RE, Raine CS, Schubart UK. Stathmin-deficient mice develop an age-dependent axonopathy of the central and peripheral nervous systems. The American journal of pathology. 2002;160(2):469-80.
15. Klim JR, Williams LA, Limone F, Guerra San Juan I, Davis-Dusenbery BN, Mordes DA, et al. ALS-implicated protein TDP-43 sustains levels of STMN2, a mediator of motor neuron growth and repair. Nat Neurosci. 2019;22(2):167-79.
16. Xiong Y, Zhao K, Wu J, Xu Z, Jin S, Zhang YQ. HDAC6 mutations rescue human tau-induced microtubule defects in Drosophila. Proc Natl Acad Sci U S A. 2013;110(12):4604-9.
17. Wittmann CW, Wszolek MF, Shulman JM, Salvaterra PM, Lewis J, Hutton M, et al. Tauopathy in Drosophila: neurodegeneration without neurofibrillary tangles. Science. 2001;293(5530):711-4.
18. Mosavi LK, Cammett TJ, Desrosiers DC, Peng ZY. The ankyrin repeat as molecular architecture for protein recognition. Protein science : a publication of the Protein Society. 2004;13(6):1435-48.

19. Musco G, Kharrat A, Stier G, Fraternali F, Gibson TJ, Nilges M, et al. The solution structure of the first KH domain of FMR1, the protein responsible for the fragile X syndrome. Nature structural biology. 1997;4(9):712-6.
20. Garcia-Mayoral MF, Hollingworth D, Masino L, Diaz-Moreno I, Kelly G, Gherzi R, et al. The structure of the C-terminal KH domains of KSRP reveals a noncanonical motif important for mRNA degradation. Structure (London, England : 1993). 2007;15(4):485-98.
21. Grishin NV. KH domain: one motif, two folds. Nucleic acids research. 2001;29(3):638-43.
22. Hollingworth D, Candel AM, Nicastro G, Martin SR, Briata P, Gherzi R, et al. KH domains with impaired nucleic acid binding as a tool for functional analysis. Nucleic acids research. 2012;40(14):6873-86.
23. Smith RK, Carroll PM, Allard JD, Simon MA. MASK, a large ankyrin repeat and KH domain-containing protein involved in Drosophila receptor tyrosine kinase signaling. Development (Cambridge, England). 2002;129(1):71-82.
24. Kallappagoudar S, Varma P, Pathak RU, Senthilkumar R, Mishra RK. Nuclear matrix proteome analysis of Drosophila melanogaster. Mol Cell Proteomics. 2010;9(9):2005-18.
25. Muller H, Schmidt D, Steinbrink S, Mirgorodskaya E, Lehmann V, Habermann K, et al. Proteomic and functional analysis of the mitotic Drosophila centrosome. EMBO J. 2010;29(19):3344-57.
26. Sansores-Garcia L, Atkins M, Moya IM, Shahmoradgoli M, Tao C, Mills GB, et al. Mask is required for the activity of the Hippo pathway effector Yki/YAP. Current biology : CB. 2013;23(3):229-35.
27. Sidor CM, Brain R, Thompson BJ. Mask proteins are cofactors of Yorkie/YAP in the Hippo pathway. Current biology : CB. 2013;23(3):223-8.
28. Traina F, Favaro PM, Medina Sde S, Duarte Ada S, Winnischofer SM, Costa FF, et al. ANKHD1, ankyrin repeat and KH domain containing 1, is overexpressed in acute leukemias and is associated with SHP2 in K562 cells. Biochimica et biophysica acta. 2006;1762(9):828-34.
29. Dhyani A, Duarte AS, Machado-Neto JA, Favaro P, Ortega MM, Olalla Saad ST. ANKHD1 regulates cell cycle progression and proliferation in multiple myeloma cells. FEBS letters. 2012;586(24):4311-8.
30. Zhu M, Zhang S, Tian X, Wu C. Mask mitigates MAPT- and FUS-induced degeneration by enhancing autophagy through lysosomal acidification. Autophagy. 2017;13(11):1924-38.
31. Akhmanova A, Steinmetz MO. Control of microtubule organization and dynamics: two ends in the limelight. Nature reviews Molecular cell biology. 2015;16(12):711-26.
32. Roux KJ, Kim DI, Burke B, May DG. BioID: A Screen for Protein-Protein Interactions. Current protocols in protein science. 2018;91:19.23.1-19.23.15.
33. Roux KJ, Kim DI, Raida M, Burke B. A promiscuous biotin ligase fusion protein identifies proximal and interacting proteins in mammalian cells. Journal of Cell Biology. 2012;196(6):801-10.
34. Branon TC, Bosch JA, Sanchez AD, Udeshi ND, Svinkina T, Carr SA, et al. Efficient proximity labeling in living cells and organisms with TurboID. Nature biotechnology. 2018;36(9):880-7.
35. Karpova N, Bobinnec Y, Fouix S, Huitorel P, Debec A. Jupiter, a new Drosophila protein associated with microtubules. Cell motility and the cytoskeleton. 2006;63(5):301-12.
36. Mitchison T, Kirschner M. Dynamic instability of microtubule growth. Nature. 1984;312(5991):237-42.
37. Chauvin S, Sobel A. Neuronal stathmins: a family of phosphoproteins cooperating for neuronal development, plasticity and regeneration. Progress in neurobiology. 2015;126:1-18.
38. Pecqueur L, Duellberg C, Dreier B, Jiang Q, Wang C, Pluckthun A, et al. A designed ankyrin repeat protein selected to bind to tubulin caps the microtubule plus end. Proc Natl Acad Sci U S A. 2012;109(30):12011-6.

536 39. Stephan R, Goellner B, Moreno E, Frank CA, Hugenschmidt T, Genoud C, et al. Hierarchical
537 Microtubule Organization Controls Axon Caliber and Transport and Determines Synaptic Structure and
538 Stability. Developmental cell. 2015;33(1):5-21.
539 40. Brooks AN, Duff MO, May G, Yang L, Bolisetty M, Landolin J, et al. Regulation of alternative
540 splicing in Drosophila by 56 RNA binding proteins. Genome research. 2015;25(11):1771-80.
541 41. Chabu C, Doe CQ. Dap160/intersectin binds and activates aPKC to regulate cell polarity and cell
542 cycle progression. Development. 2008;135(16):2739.
543 42. Budnik V, Koh YH, Guan B, Hartmann B, Hough C, Woods D, et al. Regulation of synapse
544 structure and function by the Drosophila tumor suppressor gene dlg. Neuron. 1996;17(4):627-40.
545 43. Zhu M, Li X, Tian X, Wu C. Mask loss-of-function rescues mitochondrial impairment and muscle
546 degeneration of Drosophila pink1 and parkin mutants. Human molecular genetics. 2015;24(11):3272-85.
547 44. Daniels RW, Collins CA, Gelfand MV, Dant J, Brooks ES, Krantz DE, et al. Increased expression of
548 the Drosophila vesicular glutamate transporter leads to excess glutamate release and a compensatory
549 decrease in quantal content. J Neurosci. 2004;24(46):10466-74.

550

551

552

553 **Figure Legends**

554 **Figure 1: *mask* negatively regulates microtubule stability in larval muscle and enhances**

555 **Tau-induced MT fragmentation.**

556 (**A**) Representative confocal images of microtubule (MT) in muscle 6 of wild type, *mask* null

557 ($mask^{10.22/Df}$), rescue of *mask* null with a UAS-Mask transgene driven by a muscle-specific 24B-

558 Gal4 line, and 24B-Gal4-driven UAS-*mask* RNAi. MTs are immunostained with an anti-

559 Acetylated Tubulin (Ace-Tub) antibody. Yellow dash lines denote the edge of muscle nuclei.

560 Scale bar: 5µm. (**B**) Quantification of average MT lengths. (**C**) Representative confocal images

561 of MT in muscle 6 of wild type, 24B-Gal4-driven UAS-human Tau (hTau) with UAS-Td-

562 Tomato, UAS-*mask* RNAi, or UAS-Mask. MTs are immunostained with an anti-Acetylated

563 Tubulin (Ace-Tub) antibody. Scale bar: 5µm. (**D**) Quantification of average MT lengths.

564 **Figure 2: Mask promotes normal NMJ terminal growth by regulating motor neuron**

565 **microtubule stability.**

566 (**A**) Representative confocal images of muscle 4 NMJs in wild type, *mask* null ($mask^{10.22/Df}$),

567 rescues of *mask* null with a UAS-Mask transgene driven by by pan-neuron (BG380), ubiquitous

568 (DA) or muscle (MHC) Gal4 lines, respectively, and *stathmin*/*mask* double mutant ($stai^{B200/L27}$;

569 $mask^{10.22/Df}$). Scale bar: 10 µm. (**B**) quantification of the number of boutons, synaptic span and

570 the number of branching points at the M4 NMJs. Each data point was normalized to the size of

571 the muscle 4. (**C**) Representative confocal images of segmental nerves immunostained with an

572 anti-GFP antibody in 3rd instar larvae of Elav-driven UAS-EB1-GFP with UAS-vector or UAS-

573 *mask* RNAi. Scale bar: 20 µm. (**D**) Quantification of average number of EB1-GFP puncta
574 normalized by nerve area.

575 **Figure 3: Genetic interactions between *mask* and *stai*.** (**A, B**) Loss of *stai* function suppresses
576 synaptic terminal over-expansion caused by mask loss-of-function in a dose-dependent manner.
577 (**A**) Representative confocal images of muscle 4 NMJs in larvae with Elav-driven UAS-vector,
578 Elav-driven UAS-*mask* RNAi in wild type background, *stai* heterozygous ($stai^{B200/+}$) or *stai*
579 ($stai^{B200/L27}$) homozygous mutant backgrounds. Scale bar, 10 µm. (**B**) quantification of the
580 number of boutons, synaptic span and the number of branching points at the M4 NMJs. Each
581 data point was normalized to the size of the muscle 4. NMJs are immunostained with anti-HRP
582 (red) and anti-DVGlut (green) antibodies. (**C, D, E**) Loss of *mask* function in neurons suppresses
583 *stai* mutant defects in NMJ development and axonal transport**.** (**C, D**) Representative confocal
584 images of muscle 4 NMJs (C) and lateral nerve bundles (D) in wild type, *stai* ($stai^{B200/L27}$),
585 *stai*/*mask* double mutant ($stai^{B200/L27}$;$mask^{10.22/Df}$), or *stai* mutant with pan-neuronal expression of
586 *mask* RNAi. Larval NMJs were immunostained with anti-DVGlut (green), anti-DLG (red), and
587 anti-HRP (blue). Arrows point to synaptic boutons that have postsynaptic DLG staining but lack
588 presynaptic DVGLut staining (so-called ghost boutons). Brackets highlight lateral axons that
589 shows residual DVGlut staining. Scale bars, 10 µm for C; 5 µm for D. (E) Quantification of the
590 number of ghost boutons in muscle 4 NMJs at segment A3 and A4, and axonal accumulation of
591 DVGlut.

592 **Figure 4, Loss of *mask* enhanced MT polymerization in fly larval muscle lysates.**

593 (**A**) Western analysis of total proteins and ultracentrifugal fractions (supernatant and pellet) in
594 larval muscle lysates from wild type control or *mask* knockdown (24B-Gal4-driven *mask* RNAi).

595 Lysates were treated with either 100 µm or 100 nm Taxol. Anti-beta-Tubulin and anti-alpha-
596 Actin blots were performed on total and ultracentrifugal fractions of both lysates. Anti-Mask blot
597 was preformed on lysates treated with 100 nm Taxol. The asterisks indicate the endogenous
598 Mask protein band. (**B**) Quantification of the relative levels of polymerized Tubulin in the pellet
599 fraction in the lysate treated by 100 nm Taxol. The levels of polymerized Tubulin were
600 normalized to the levels of total Tubulin. Error bars indicate SEM. n = 3 trials.

601 **Figure 5, Rescue experiments identify structural requirement for Mask's action in**
602 **regulating MT stability.**

603 (A) A schematic of wild type and modified UAS-Mask transgenes used in the rescue
604 experiments and representative western blots showing muscle expression of Mask in wild type,
605 *mask* null mutant, as well as *mask* null expressing each of the four UAS-Mask transgenes in
606 muscles. Note that the anti-Mask antibody does not recognize GFP-Mask-KH-Only protein,
607 indicating the antigen of this antibody is outside of the Mask-KH-Only region. Anti-GFP western
608 blots were performed to show GFP-Mask-KH-Only (as indicated by an asterisk). (B)
609 Representative confocal images of MT in muscle 6 of wild type, *mask* null ($mask^{10.22/Df}$), rescues
610 of *mask* null with MHC-Gal4-driven UAS-Mask, UAS-Mask-KH, UAS-Mask-KH-Only, or
611 UAS-Mask-ANK. Scale bar: 10 µm. (C) Quantification of average MT lengths. (D)
612 Representative confocal images of muscle 4 NMJs in wild type, *mask* null ($mask^{10.22/Df}$), rescues
613 of *mask* null with pan-neuron (BG380) driven wild type or modified UAS-Mask transgenes as
614 shown in A. Scale bar: 10 µm. (E) quantification of the number of boutons, synaptic span and the
615 number of branching points at the M4 NMJs. Each data point was normalized to the size of the
616 muscle 4.

**Figure 6, Mask interacts with Jupiter and regulates its localization to microtubules.**

(**A**) Representative western blots showing co-IP of endogenous Mask and mCh-Jupiter in lysates from larval brains. Note that Mask protein undergo certain degree of degradation after immunoprecipitation as indicated by faster migration in SDS-PAGE. **(D, F)** Representative confocal images of segmental nerves (D), or muscle 4 NMJs (F), immune-stained with anti-mCherry (Red) and anti-Futsch (gree) antibodies in 3$^{rd}$ instar larvae of Elav-driven UAS-mCh-Jupiter with UAS-control RNAi, UAS-mask RNAi or UAS-Mask. (**E, G**) Quantification of mean intensity of mCherry and Futsch. Scale bars: 10 μm.

Supplement Figure 1, Mask regulates the abundance of Tau protein in larval muscles.

(A) Representative confocal images of hTau expression in muscle 6 of 24B-Gal4-driven UAS-human Tau (hTau) with UAS-Td-Tomato, UAS-*mask* RNAi, or UAS-Mask. Human Tau proteins are immunostained with an anti-Tau antibody. Scale bar: 10 μm. (B) Quantification of mean intensity of hTau expression levels.

**Supplement Figure 1, Mask regulates the abundance of Tau protein in larval muscles.**

(A) Representative confocal images of hTau expression in muscle 6 of 24B-Gal4-driven UAS-human Tau (hTau) with UAS-Td-Tomato, UAS-*mask* RNAi, or UAS-Mask. Human Tau proteins are immunostained with an anti-Tau antibody. Scale bar: 10 μm. (B) Quantification of mean intensity of hTau expression levels.

# Figure 1

A

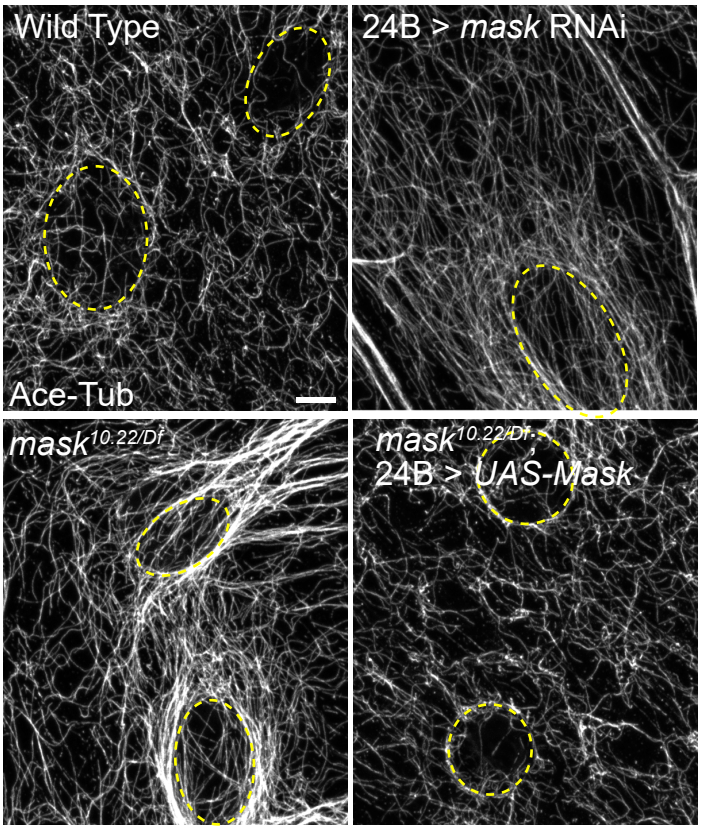


B

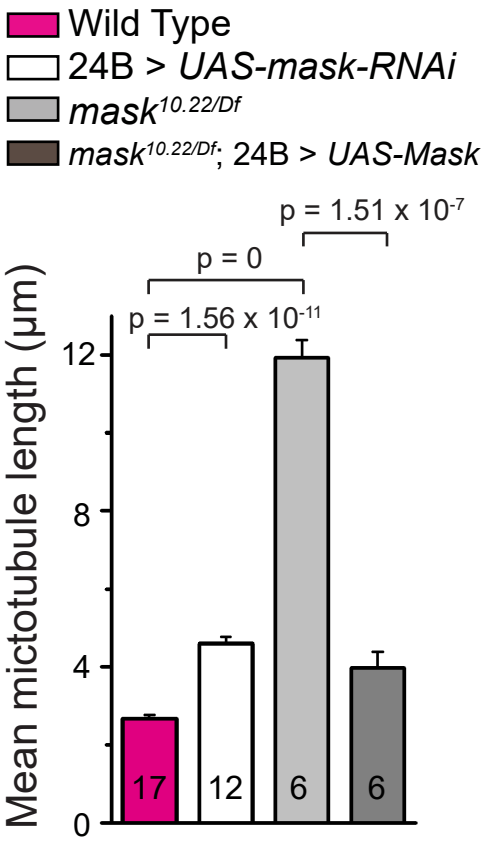


C

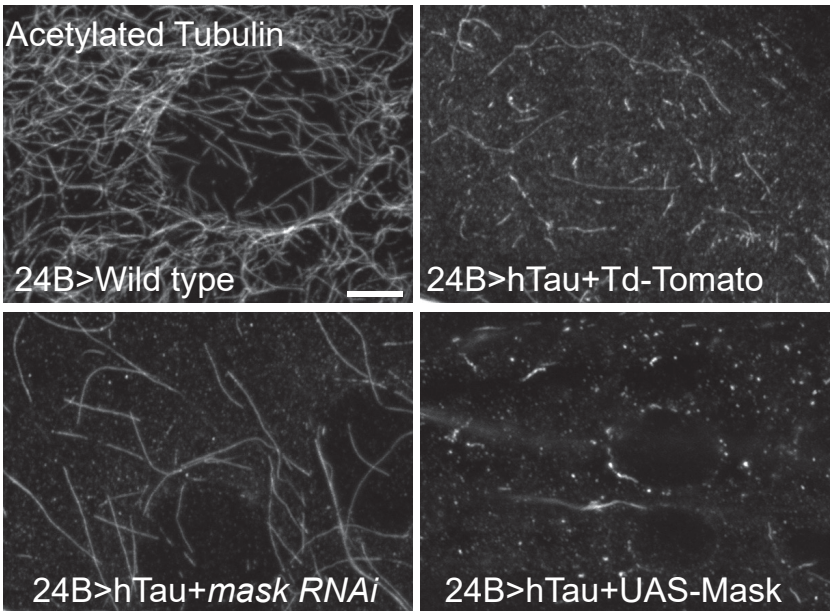


D

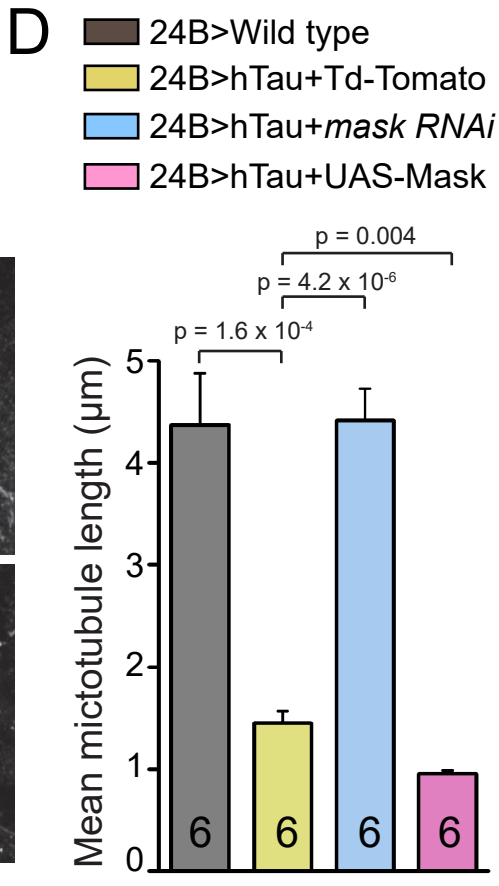

# Figure 2

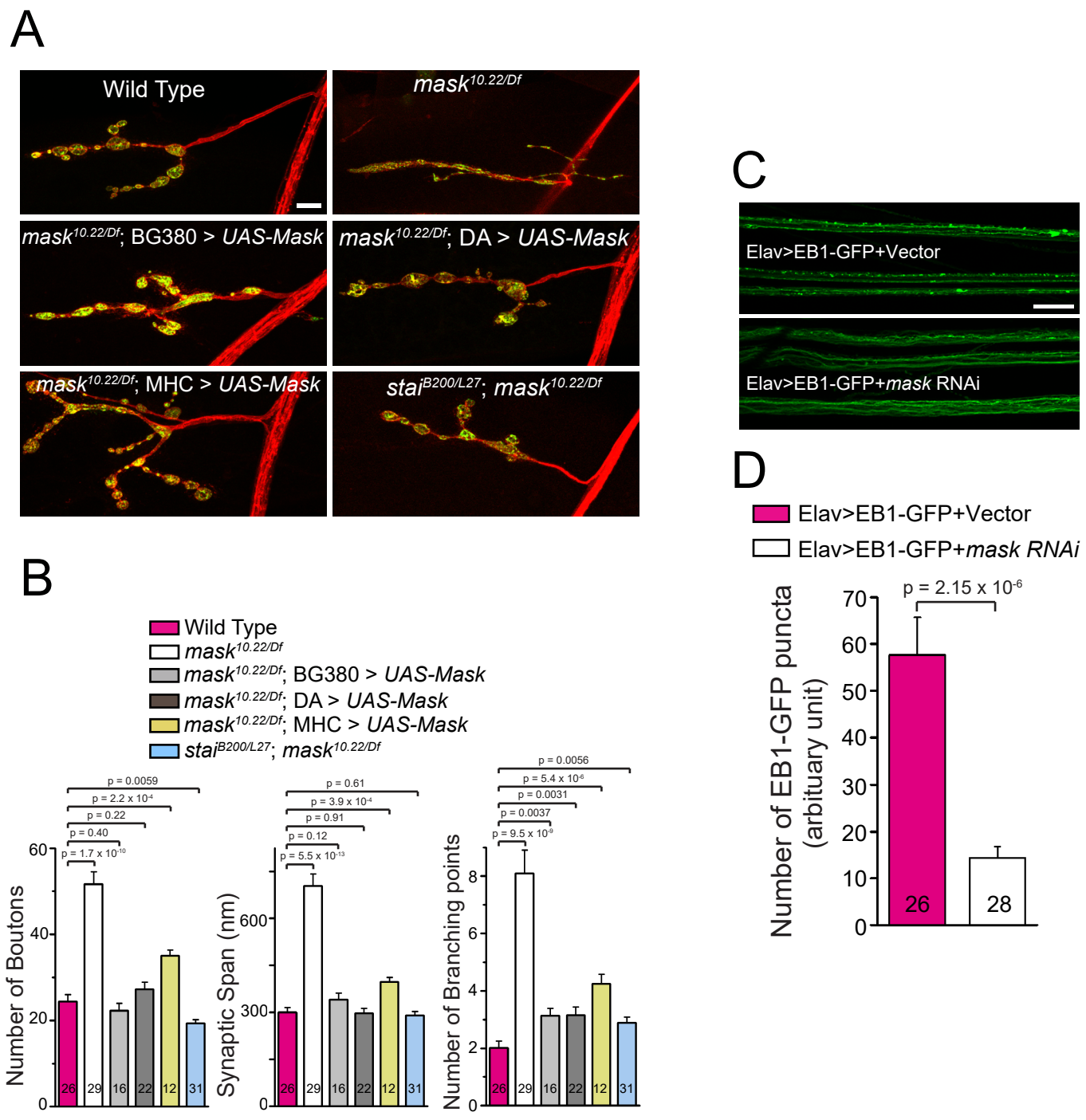

# Figure 3

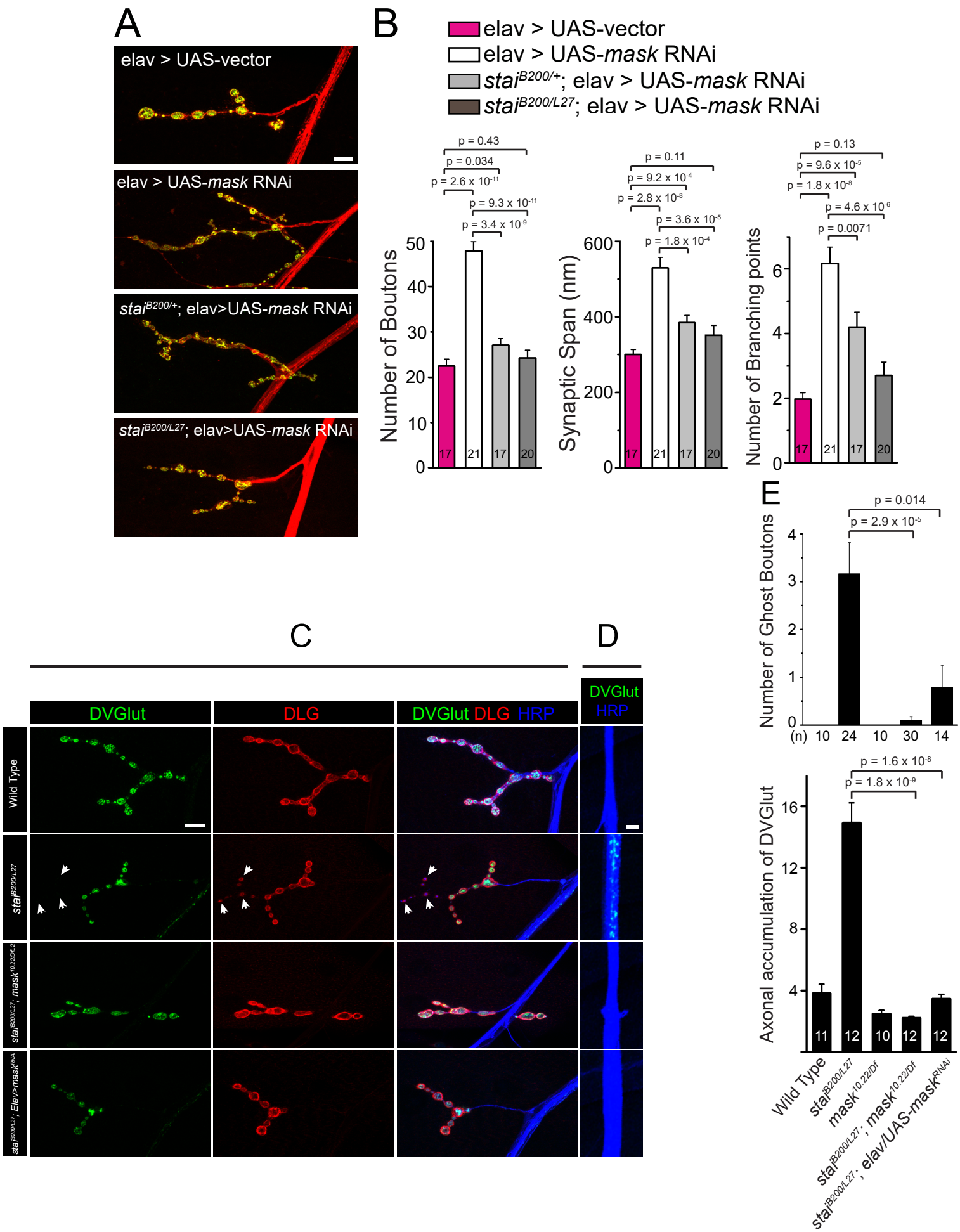

# Figure 4

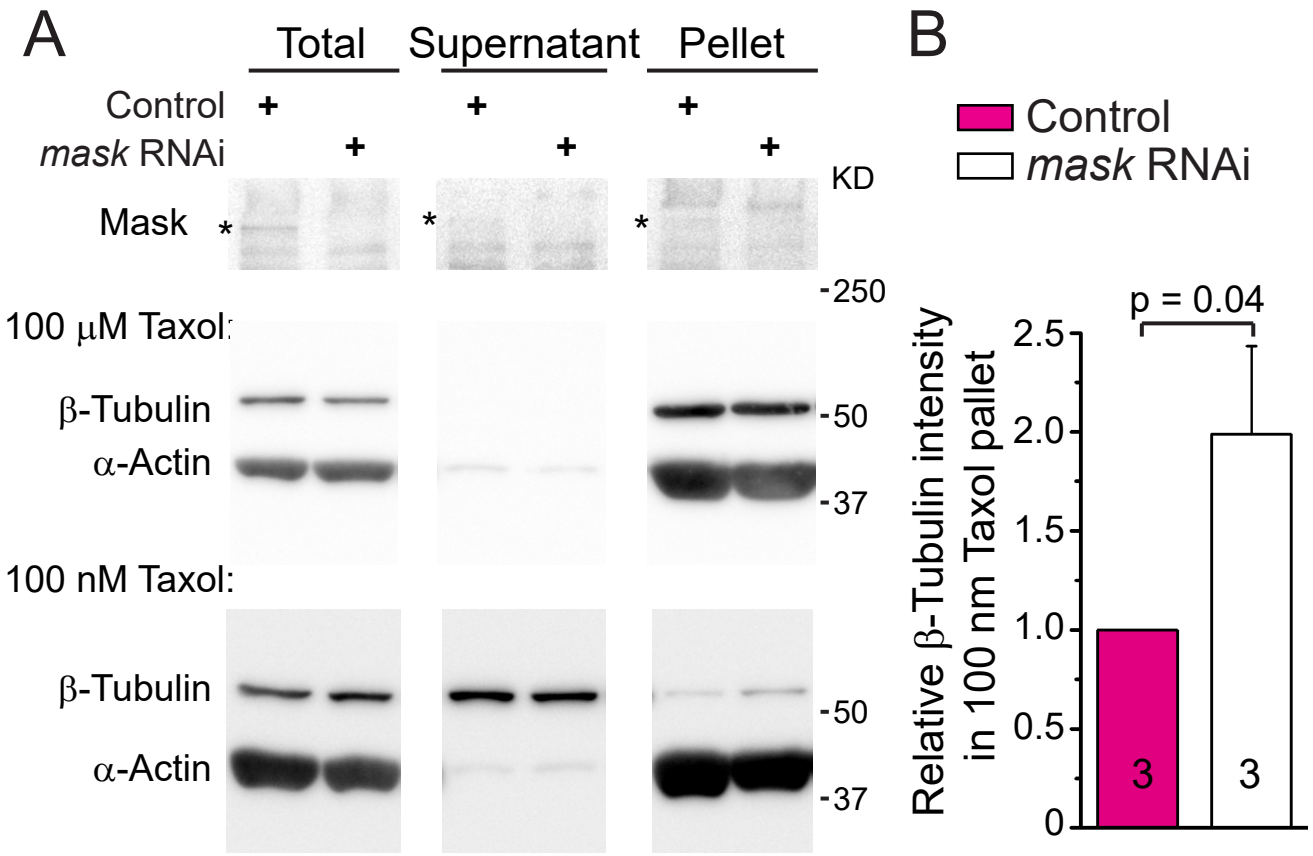

# Figure 5

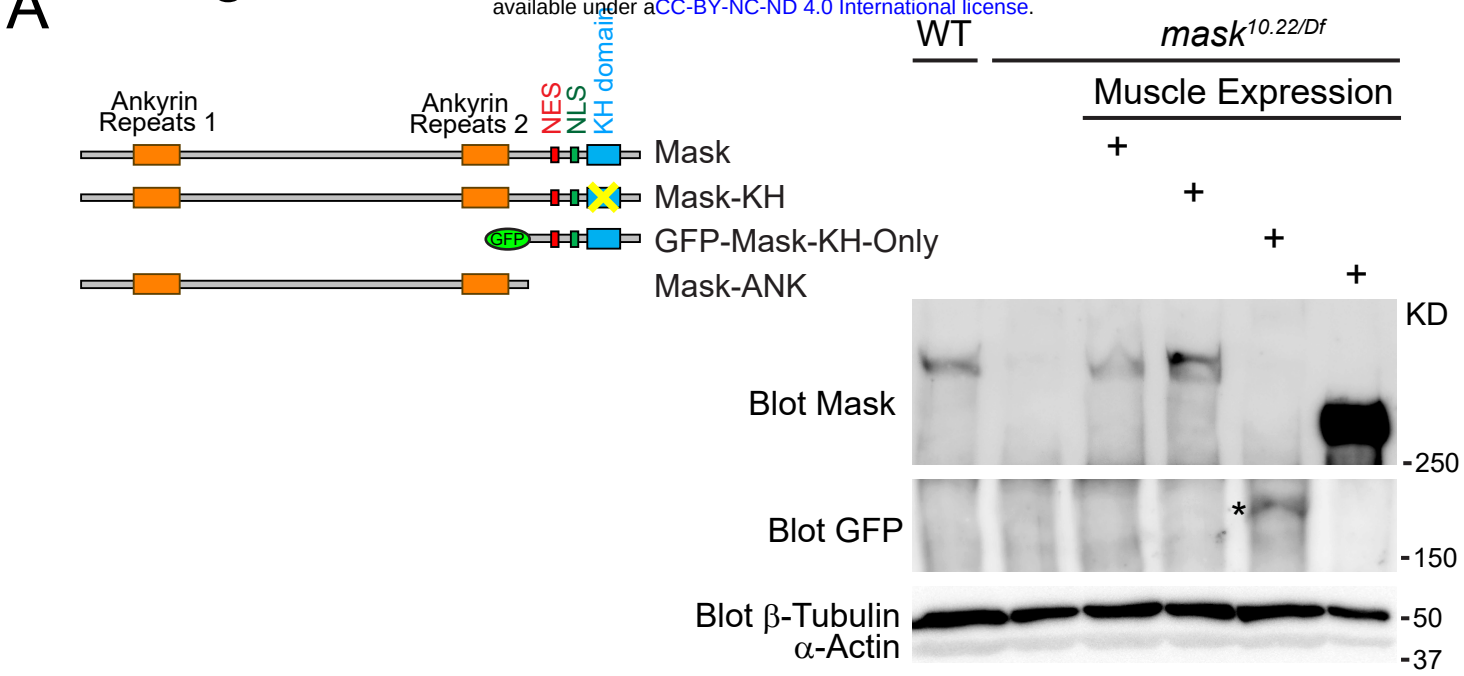


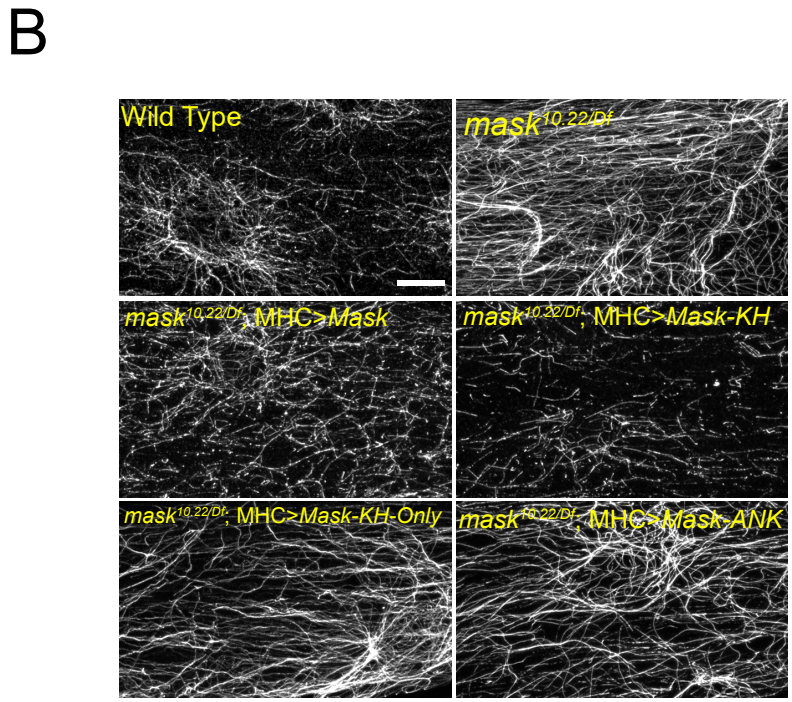


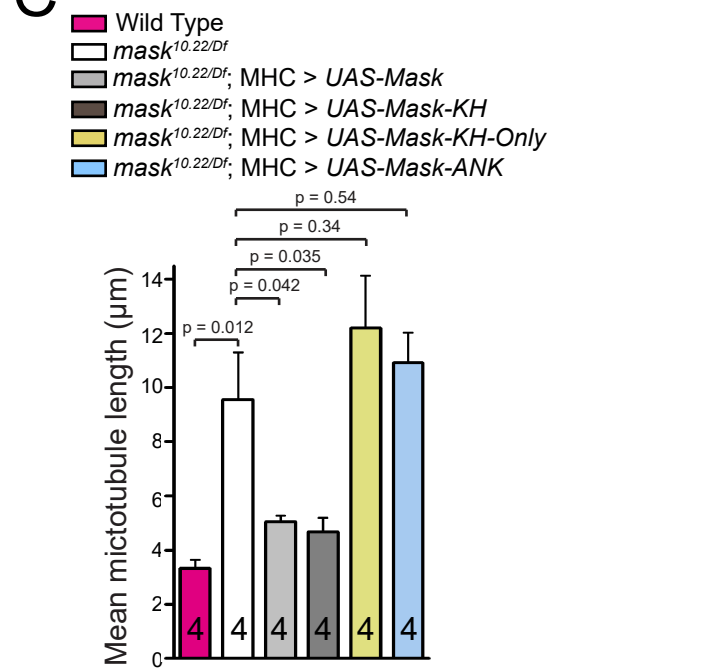


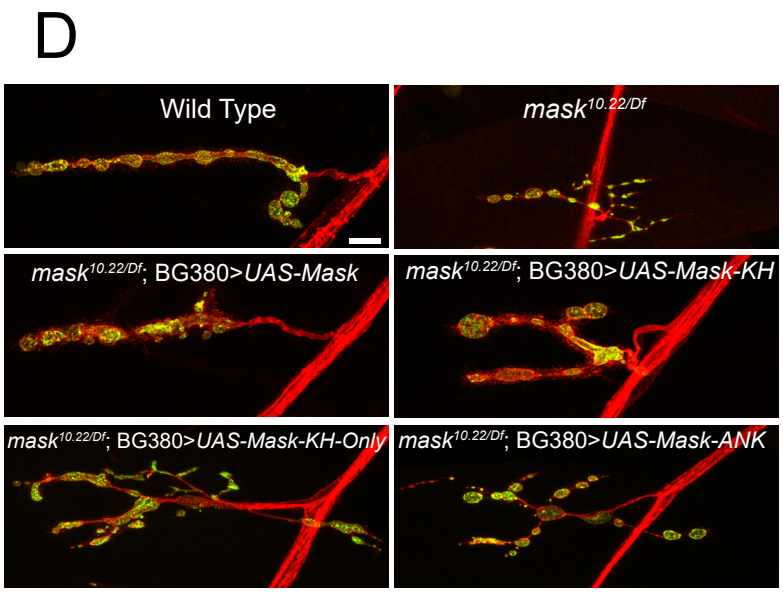


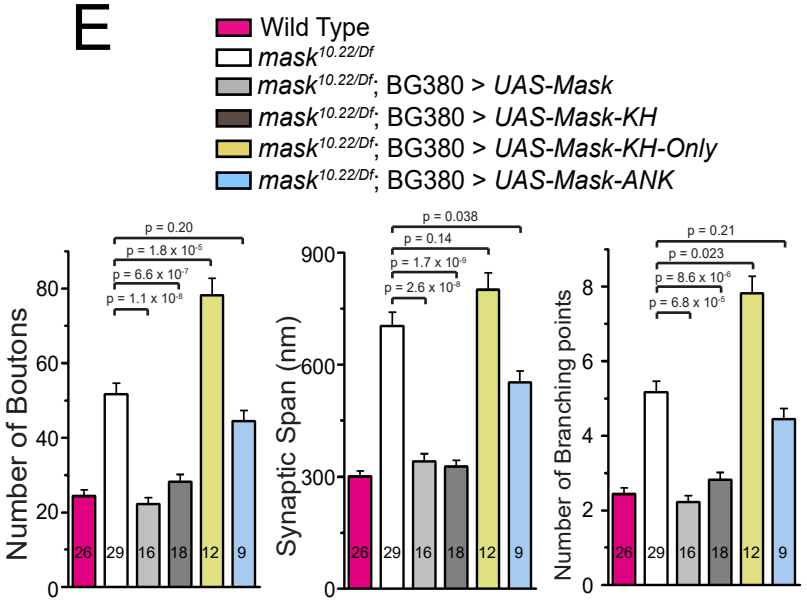

# Figure 6